Ji X, Zhang J, Ikago K, et al. Tuned viscous mass damper (TVMD) coupled wall system for enhancing seismic performance of high-rise buildings[J]. Engineering Structures, 2021, 240: 112307.

Tuned Viscous Mass Damper (TVMD) Coupled Wall System for Enhancing Seismic Performance of High-Rise Buildings

Xiaodong Ji[a], Junshan Zhang[a], Kohju Ikago[b], Sanjukta Chakraborty[a], Hideto Kanno[c]

[a]*Key Laboratory of Civil Engineering Safety and Durability of China Education Ministry, Department of Civil Engineering, Tsinghua University, Beijing 100084, China*

[b]*International Research Institute of Disaster Science, Tohoku University, Sendai, 980-0845, Japan*

[c]*Graduate School of Systems Science and Technology, Akita Prefectural University, Yurihonjo 015-0055, Japan*

Abstract: This paper proposes an innovative coupled wall system, named 'the tuned viscous mass damper (TVMD) coupled wall system' for use in high-rise buildings. This novel wall system is expected to control both lateral inter-story drifts and floor accelerations of high-rise buildings when subjected to strong ground motions, thus enhancing their seismic resilience. The TVMD consists of a component that provides stiffness connected in series with a ball screw device that can provide large inertial and damping forces, even when subjected to small deformations. In this system, TVMDs are arranged to connect adjacent wall piers in a zig-zag configuration. Such a strategic arrangement of TVMDs makes efficient use of the vertical relative displacements of the adjacent walls induced by their flexural deformation to generate the motions and forces of the TVMDs. Two methods are presented for optimal design of this system, namely the single-mode tuning method and multi-mode tuning method. Dynamic response analysis is conducted on a representative 15-story TVMD coupled wall system. Results of the analysis indicate that the TVMDs designed by the single-mode tuning method

not only suppress the dynamic responses of the tuning mode, but also provide additional damping for the lower-order modes of the primary structure. The multi-mode tuning method shows similar performance to the single-mode tuning method, if the latter is used to tune the higher-order mode. Finally, real-time hybrid simulations were conducted to examine the seismic performance of the proposed system. The test results demonstrate the benefit of the TVMD coupled wall system, and indicate that the detuning effect is slight for this system even subjected to strong ground motions.

Keywords: tuned viscous mass damper (TVMD); coupled wall system; seismic response control; optimum design; real-time hybrid simulation; high-rise buildings

1. Introduction

Recent earthquake disasters in urban regions highlight two major challenges for high-rise buildings in terms of earthquake resilience. The first challenge is that severe damage to structural components, which is primarily induced by large inter-story drifts, is difficult to repair, particularly in members with large gravity loads. As a result, a large number of high-rise buildings are demolished after earthquakes (e.g., the 2011 Canterbury earthquake), despite not collapsing during the earthquake [1]. The second challenge is that severe damage to non-structural components leads to significant loss of functionality and consequently results in prolonged downtime [2]. Such damage is primarily caused by large accelerations of upper floors, particularly when the high-rise buildings are subjected to long-period, long-duration ground motion (for example, the 2011 Tohoku-Oki earthquake) [3]. As such, control of both inter-story drifts and floor accelerations is necessary for enhancing the seismic resilience of high-rise buildings.

Reinforced concrete (RC) shear wall system is often used for high-rise buildings to provide adequate lateral stiffness and strength for resisting wind loads and earthquake actions. To effectively control the seismic responses of the RC wall structures, the addition of dampers or energy dissipators is a recognized solution. In recent, the efforts have been devoted to development of coupling beam dampers used for RC wall systems, for example, replaceable steel coupling beams [4,5,6], friction coupling beams [7] and viscoelastic coupling beams [8]. Among them, the replaceable steel coupling beams, which include a shear link or shear-type metallic dampers, appear to be most promising, and they have seen increased use in regions of high seismicity. Nevertheless, past research [9] indicates that although the replaceable steel coupling beams can significantly decrease the inter-story drifts of high-rise buildings subjected to severe ground motions, they cannot effectively control the floor accelerations.

This paper proposes an innovative coupled wall system (see Fig. 1), named the tuned viscous mass damper (TVMD) coupled wall system, for achieving simultaneous control of the inter-story drifts and floor accelerations of high-rise buildings. Three highlights are included in the development of this system. (1) TVMD devices, which can generate large inertial and damping forces even under a small deformation by use of ball screw mechanism [10,11], are adopted in this system. (2) TVMDs are arranged between two adjacent wall piers in a zig-zag configuration. Such a strategic configuration makes efficient use of the vertical relative displacements of the adjacent walls induced by their flexural deformation to generate the forces of the TVMDs. (3) The optimal design of the parameters of TVMDs along the structural height, including apparent mass (i.e., inertance produced by an inerter [12]), stiffness and damping coefficient, is developed for this system for effective control of the seismic responses.

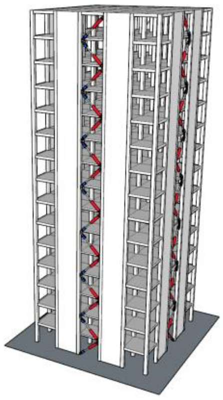

Fig. 1. Schematic drawing of TVMD coupled wall system.

The TVMD belongs to the inerter-based vibration absorbers, where the inerter represents a two-terminal mechanical element developing a resisting force proportional to the relative acceleration of its terminals, with proportionality constant express in mass units and termed “inertance” [12]. The interter can be realized by the mechanical devices with a ball screw system [10,11], a rack-and-pinion flywheel system [13], hydraulic devices [14,15] and electromagnetic devices with capacitors [16,17]. Various configurations of interter, spring, and viscous damper (dashpot) elements forms different inerter-based vibration absorbers, including the TVMD, tuned inerter damper (TID) [18] and tuned mass damper inerter (TMDI) [19]. These inerter-based vibration absorbers have shown promising capability in suppressing vibration and seismic responses of structures, e.g., bridge cables [20,21], base isolated structures [22] and high-rise buildings [23].

For application of the inerter-based vibration control techniques, significant efforts have been devoted to develop the optimal tuning design methods for determining the parameters of the inerter-based vibration absorbers. Ikago et al. [11] proposed a fixed-point tuning design method of TVMD that can achieve the H_∞ optimization of the transfer function of a single-degree-of-freedom (SDOF) primary structure. Marian et al. [19] proposed a method for the TMDI design, based on the H_2 optimization of the white-noise excited response of a SDOF primary structure. While the aforementioned optimal methods provide explicit design equations and can be extended for use in tuning a single-mode response of a multi-degree-of-freedom (MDOF) structure [24,25,26], they are not suitable for optimization of multi-mode responses of a MDOF system. Therefore, the numerical optimization methods [23,27,28,29] were developed for minimization of seismic dynamic responses or transfer functions of MDOFs. More recently, multiple objectives are considered in the numerical optimization. For example, Pan et al. [30] proposed to optimal design of inerter-based type dampers by minimization of both structural response and damper forces that represents the device costs. Ruiz et al. [31] and Taflanidis et al. [32] proposed the optimal design in consideration of the compromise among multiple objectives, e.g., the life-cycle cost of the system, repair cost, inerter force, and structural seismic responses. While the numerical optimization methods can provide improved results, they are much computational demanding compared to the explicit optimal design equations.

The objective of this paper is to present the concept of the TVMD coupled wall system and develop the optimal design methods of this system. Numerical analyses using a simplified model and real-time hybrid tests on a small-scale model were carried out to demonstrate the characteristic and advantages of this system. The paper is structured as follows. The second section presents the concept of the TVMD coupled wall system, and develops the numerical model of a representative TVMD coupled wall. The third section proposes a single-mode tuning method for optimal design of the TVMD coupled wall system. The fourth section describes a multi-mode tuning method, in which sequential quadratic programming (SQP) optimization is used for optimal design of the system for controlling multiple modes of vibration. Finally, real-time hybrid simulations were conducted to examine the performance of the proposed system subjected to various intensities of ground motions. The simulation also indicates that the detuning effect is slight for the TVMD coupled wall system even when subjected to severe seismic motions.

2. Concept and modelling of TVMD coupled wall system

2.1. Tuned viscous mass damper (TVMD)

The TVMD was developed from a rotary damping tube (RDT) that is equipped with a rotary tube filled with viscous fluid and a rotary cylinder acting as a flywheel [33]. By using the ball screw, this damper can transfer its axial deformation to high-speed rotation of the tube and flywheel, and thus provide amplified damping force and inertial force, respectively. As a further development, Saito [10] and Ikago [11] added a spring connected in series to the RDT as a stiffness device, to form the so-named ‘tuned viscous mass damper (TVMD)’. As shown in Fig. 2, the mechanical model of a TVMD consists of an inerter element (functioning from the rotary flywheel), the viscous damper element (functioning from the rotary tube with viscous fluid), and an in-series connected stiffness element (functioning from the spring). Therefore, these elements parameters, including the stiffness k_b, damping coefficient c_d, and apparent mass m_r can be designed to tune the vibration of primary structure, in a similar way to a tuned mass damper (TMD). Note that the apparent mass m_r of a TVMD can reach several hundred times of its actual mass m_f by the amplification of the ball screw mechanism. The amplification factor between the apparent mass to the actual mass is related to the outer and inner radii of the flywheel and the lead length of the ball screw [11].

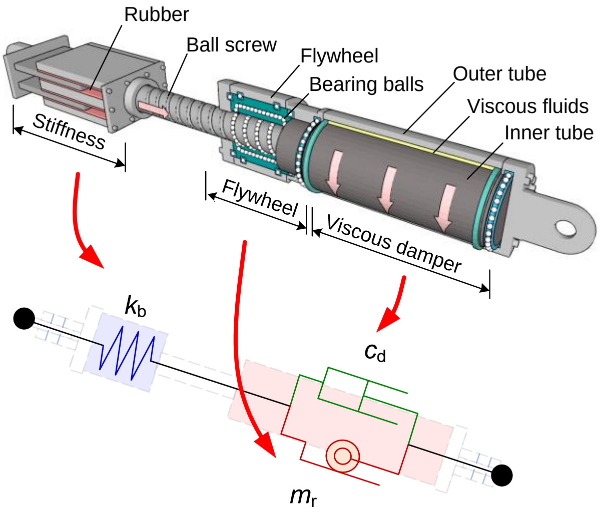

Fig. 2. Schematic drawing and mechanical model of TVMD.

2.2. TVMD coupled wall system

Fig. 3 shows the deformation mode of the TVMD coupled wall system when subjected to ground motions. The configuration of the system is expected to have the following advantages. (1) High damping force can be achieved under a small inter-story drift. During an earthquake, the flexural deformation of wall piers will result in large relative vertical displacement at the edges of two adjacent wall piers, which can generate axial deformation of TVMDs, as shown in Fig. 3. In addition, with proper tuning design, the ball screw part and the spring part deform in the opposite direction during the tuning vibration of TVMD (the mechanism will be discussed in Subsection 3.2), which can further increase the deformation of the ball screw device. As such, the deformation of the inerter and viscous damper may be several times greater than the lateral drift of the story where the TVMD is installed. (2) The joints between TVMD and wall pier are easy to design. At the joint (see Fig. 3), one TVMD provides the tensile force and another provides the compressive force. As a result, the resultant vertical force at the joint provides the coupling action to the wall piers, while the resultant horizontal force applied to the joint would be small.

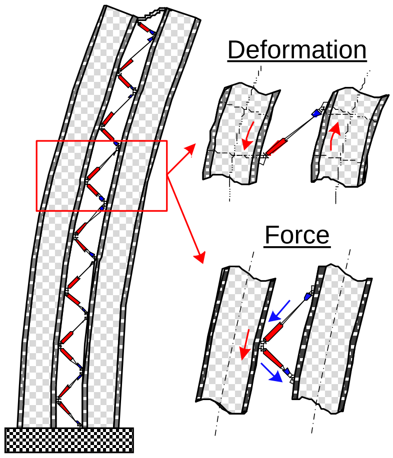

Fig. 3. Deformation pattern and joint force.

2.3. Prototype structure

To investigate the design method and seismic performance of the TVMD coupled wall system, a virtual 15-story commercial office building is adopted for analysis. The total height of the structure is 67.5 m with a uniform story height of 4.5 m. The prototype structure uses the RC frame-shear wall system. A representative floor plan of the structure is shown in Fig. 4(a), with plan dimensions of 25 m × 18 m. The building is assumed to be located in Beijing, where the peak ground acceleration (PGA) is 0.2 g for the design basis earthquake (DBE, with a probability of exceedance of 10% in 50 years) and the characteristic site period T_g is 0.45 s.

The structure without TVMDs is designed according to the Chinese code for seismic design of buildings (GB 50011-2010) [34] and Chinese technical specification for concrete structures of tall buildings (JGJ 3-2010) [35]. It is designed to satisfy the strength demand of the service level earthquake (SLE, with a probability of exceedance of 63% in 50 years), which has a peak ground acceleration of 0.07 g. Linear response spectrum analysis of a three-dimensional structural model is performed to determine the design forces of structural components and the deformation of the structure. In this analysis, a damping ratio of 5% is assumed for all modes.

The shear walls in the longitudinal direction highlighted as a double wall system (DBW) in Fig. 4(a) are selected for further analysis. As shown in Fig. 4(b). DBW represents two isolated walls connected by floor slabs. The wall thickness varies from 400 to 300 mm along the structural height. To ensure the DBW model can reasonably capture dynamic behavior of the prototype structure, the seismic masses in the DBW are assumed to follow the floor mass distribution along the height and they are scaled such that the DBW has similar dynamic characteristics to the prototype structure in the longitudinal direction. The floor seismic mass acting on the DBW varies from 90 to 80 ton along the height, as shown in Fig. 4(b). The natural period of the first three modes of the DBW model are 2.28 s, 0.39 s, and 0.14 s. Installation of the TVMDs between the adjacent wall piers forms the TVMD coupled wall system (TCW) as shown in Fig. 4(c), which will be adopted for the following analysis.

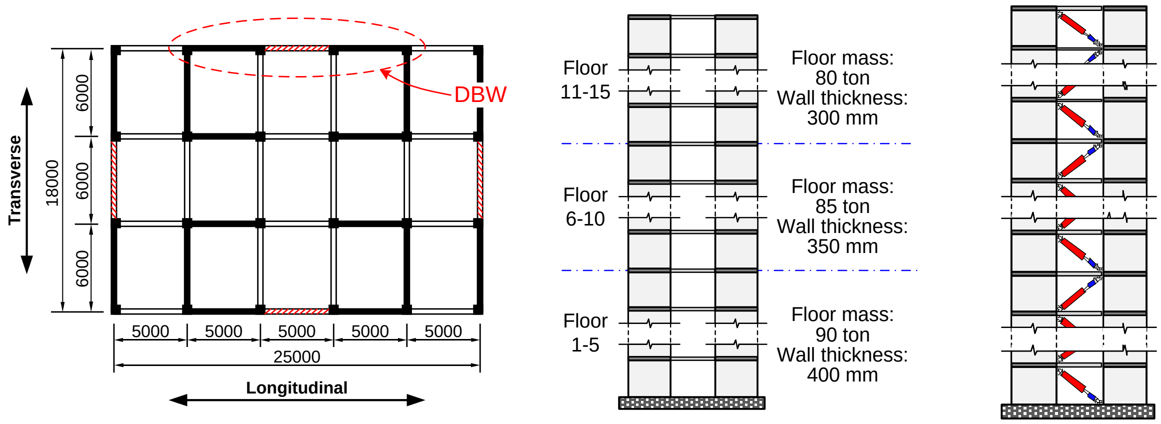

(a) Plain view of prototype structure (unit: mm)

(b) Elevation of DBW system

(c) Elevation of TCW system

Fig. 4. Prototype structure.

2.4. Numerical model for TVMD coupled wall system

For development of the optimal design method, a simplified numerical model of the TVMD coupled wall system was developed in Matlab. Fig. 5(a) shows the DBW model, where the wall pier is simulated by Timoshenko beam elements located along the centroid of the wall sections. A rigid beam element with a length equal to the wall's sectional depth is added at each floor level, to represent the rigidity of the wall along its section. Floor mass is assigned across several nodes of the wall piers at each floor level, as shown in Fig. 5(a). A rigid link element is added to connect two wall piers at each floor level to simulate the rigid diaphragm. The Rayleigh damping model is adopted, where the parameters are determined based on the assumption that the damping ratio of the first and third modes are equal to 0.05. The simplified model of the DBW in Matlab was validated by comparison with the model developed in the software SAP2000 where the wall piers were simulated by shell elements. Both models have nearly identical modal properties.

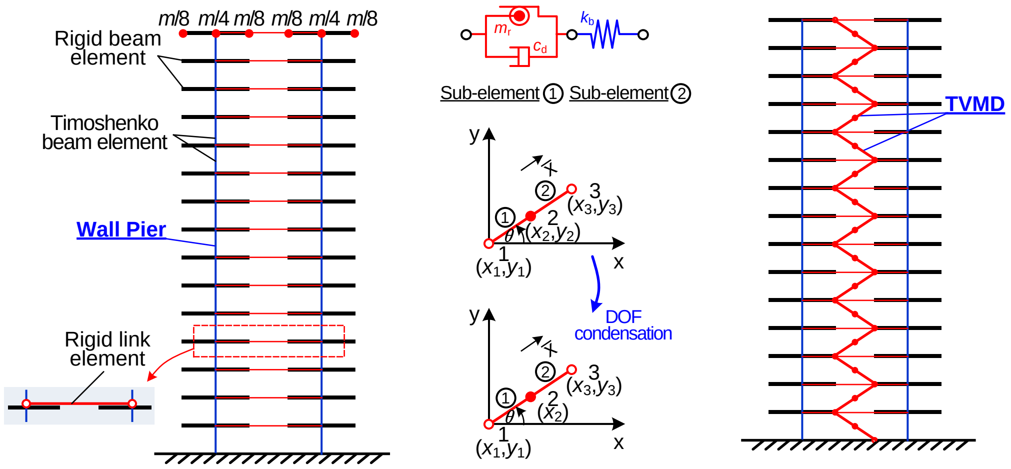

(a) DBW model (b) TVMD element (c) TCW model

Fig. 5. Numerical model of TVMD coupled wall system.

As shown in Fig. 5(b), a TVMD is simulated by two sub-elements connected in series. Sub-element 1, representing the ball screw, comprises an inerter and a dashpot connected in parallel. Sub-element 2, representing the stiffness device, consists of an elastic spring.

Because the TVMD works like a one-dimensional element and three nodes move only along the longitudinal direction of the device, a TVMD element includes 3 DOFs $\{\bar{x}_1, \bar{x}_2, \bar{x}_3\}^{\mathrm{T}}$ in the local coordinate system. The mass, damping and stiffness matrices in the local coordinate system, denoted as $[\bar{M}]^{\mathrm{e}}$, $[\bar{C}]^{\mathrm{e}}$ and $[\bar{K}]^{\mathrm{e}}$, for a TVMD element are expressed as follows.

$$[\bar{M}]^{\mathrm{e}} = \begin{bmatrix} m_{\mathrm{r}} & -m_{\mathrm{r}} & 0 \\ -m_{\mathrm{r}} & m_{\mathrm{r}} & 0 \\ 0 & 0 & 0 \end{bmatrix}, \quad [\bar{C}]^{\mathrm{e}} = \begin{bmatrix} c_{\mathrm{d}} & -c_{\mathrm{d}} & 0 \\ -c_{\mathrm{d}} & c_{\mathrm{d}} & 0 \\ 0 & 0 & 0 \end{bmatrix}, \quad [\bar{K}]^{\mathrm{e}} = \begin{bmatrix} 0 & 0 & 0 \\ 0 & k_{\mathrm{b}} & -k_{\mathrm{b}} \\ 0 & -k_{\mathrm{b}} & k_{\mathrm{b}} \end{bmatrix} \tag{1}$$

where m_{r} denotes the apparent mass of the inerter, c_{d} denotes the damping coefficient of the viscous damper, k_{b} denotes the stiffness of the spring. Afterward, the mass, damping and stiffness matrices of a TVMD in the global coordinate system (i.e., the x-y coordinate system in Fig. 5(b)), denoted as $[M]^{\mathrm{e}}$, $[C]^{\mathrm{e}}$ and $[K]^{\mathrm{e}}$, can be obtained by the coordinate transformation as follows:

$$[M]^{\mathrm{e}} = [T]^{\mathrm{T}} [\bar{M}]^{\mathrm{e}} [T], \quad [C]^{\mathrm{e}} = [T]^{\mathrm{T}} [\bar{C}]^{\mathrm{e}} [T], \quad [K]^{\mathrm{e}} = [T]^{\mathrm{T}} [\bar{K}]^{\mathrm{e}} [T] \tag{2}$$

$$[T] = \begin{bmatrix} \cos\theta & \sin\theta & 0 & 0 & 0 & 0 \\ 0 & 0 & \cos\theta & \sin\theta & 0 & 0 \\ 0 & 0 & 0 & 0 & \cos\theta & \sin\theta \end{bmatrix} \tag{3}$$

where $[T]$ denotes the coordinate transformation matric, the superscript T denotes the transpose operation, and θ denotes the rotation angle between the local and global coordinate system as shown in Fig. 5(b).

The size of the matrices $[M]^{\mathrm{e}}$, $[C]^{\mathrm{e}}$ and $[K]^{\mathrm{e}}$ are 6-by-6, corresponding to the DOFs $\{x_1, y_1, x_2, y_2, x_3, y_3\}^{\mathrm{T}}$. Considering that three nodes in a TVMD element shall be always collinear during their movement, one DOF can be eliminated using the kinematic constraints. By neglecting the slight variation of TVMD incline angle during the motion, the DOF y_2 can be expressed by other DOFs using Eq. (4).

$$\begin{Bmatrix} x_1 \\ y_1 \\ x_2 \\ y_2 \\ x_3 \\ y_3 \end{Bmatrix} = \begin{bmatrix} 1 & 0 & 0 & 0 & 0 \\ 0 & 1 & 0 & 0 & 0 \\ 0 & 0 & 1 & 0 & 0 \\ -\tan\theta & 1 & \tan\theta & 0 & 0 \\ 0 & 0 & 0 & 1 & 0 \\ 0 & 0 & 0 & 0 & 1 \end{bmatrix} \begin{Bmatrix} x_1 \\ y_1 \\ x_2 \\ x_3 \\ y_3 \end{Bmatrix}, \quad \text{i.e.} \quad \{u\} = [T_\mathrm{c}] \cdot \{u_\mathrm{c}\} \tag{4}$$

where $[T_\mathrm{c}]$ denotes the condensation matrix.

Therefore, the mass, damping and stiffness matrices of a TVMD can ben condensed into the matrices $[M]_\mathrm{c}^\mathrm{e}$, $[C]_\mathrm{c}^\mathrm{e}$ and $[K]_\mathrm{c}^\mathrm{e}$ with a size of 5-by-5, by the following equation.

$$[M]_\mathrm{c}^\mathrm{e} = [T_\mathrm{c}]^\mathrm{T} [M]^\mathrm{e} [T_\mathrm{c}], \quad [C]_\mathrm{c}^\mathrm{e} = [T_\mathrm{c}]^\mathrm{T} [C]^\mathrm{e} [T_\mathrm{c}], \quad [K]_\mathrm{c}^\mathrm{e} = [T_\mathrm{c}]^\mathrm{T} [K]^\mathrm{e} [T_\mathrm{c}] \tag{5}$$

The TCW model is constructed by integrating the TVMD elements into the DBW model, as shown in Fig. 5(c).

3. Single-mode tuning design and analysis

3.1. Single-mode tuning design method

The optimal design of TVMD is similar to the design concept of TMD, where the vibration frequency of the TMD is tuned to a target mode frequency of the primary structure for minimizing its dynamic response. The fixed point method proposed by Ormondroyd and Den Hartog [36,37] is the commonly used approach for optimal design of TMD. Ikago et al. [11] extended the fixed point method for optimal design of TVMD in a SDOF undamped or lightly damped system. Based on this method, for a given mass ratio μ, the optimal frequency $\omega_\mathrm{d}^\mathrm{opt}$ and damping ratio $\varsigma_\mathrm{d}^\mathrm{opt}$ of the TVMD are given by:

$$\omega_\mathrm{d}^\mathrm{opt} = \frac{1}{\sqrt{1-\mu}} \omega_0 \tag{6}$$

$$\varsigma_\mathrm{d}^\mathrm{opt} = \frac{1}{2} \sqrt{\frac{3\mu}{(2-\mu)}} \tag{7}$$

where ω_0 denotes the natural frequency of the primary structure, the mass ratio $\mu = m_\mathrm{r} / m$ represents the ratio of the apparent mass of TVMD m_r to the mass of the primary structure m. Note that the above optimal frequency and damping ratio obtained by Eqs. (6) and (7) correspond to the minimization of the H_∞ norm of the transfer function from the base acceleration excitation to the displacement response of the SDOF primary structure [11].

Ikago et al. [24, 25] further extended the fixed point method from a SDOF system to the optimal design of TVMDs used in shear-type multi-story frame structures. The dynamic response of a linear MDOF system can be regarded as the combined response of a series of modes, while the fixed point method is used to design TVMDs tuned to a given mode of interest. The key to success of the method is how the apparent mass of the TVMDs is assigned along the height. Ikago et al. [24, 25] recommended that the apparent mass distribution of TVMDs is proportional to the story shear stiffness for the shear-type structures (e.g., frames), where the TVMDs are mobilized by the inter-story drifts. However, this recommendation is not suitable for the coupled wall system, which belongs to a flexure-type structure. In the coupled wall system, the TVMDs are mobilized majorly by the relative vertical displacements between adjacent wall piers.

In this study, the apparent mass distribution of TVMDs in the coupled wall system is assumed to be proportional to the modal displacement demand vector of the TVMDs for the target tuning mode. For a given mode, the modal displacement demand of a TVMD is defined as the relative displacement, between the two nodes installing the TVMD, in this mode shape vector. This assumption is based on the hypothesis that a larger TVMD shall be assigned at a location with a larger deformation demand. If the *i*th mode is selected as the target tuning mode, the modal displacement demand vector of TVMDs $\{\phi_{\mathrm{d}i}\}$ can be calculated from the

ith mode shape vector of the DBW $\{\phi_i\}$ (see Fig. 6(a)). Fig. 6(b) shows the first three mode shapes of the DBW, and Fig. 6(c) shows the corresponding modal displacement demand vectors of TVMDs.

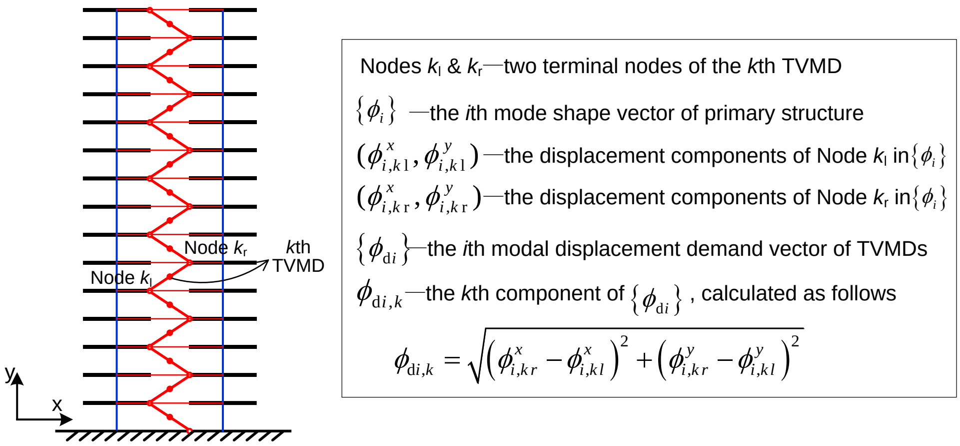

(a) Calculation of modal displacement demand vector of TVMDs

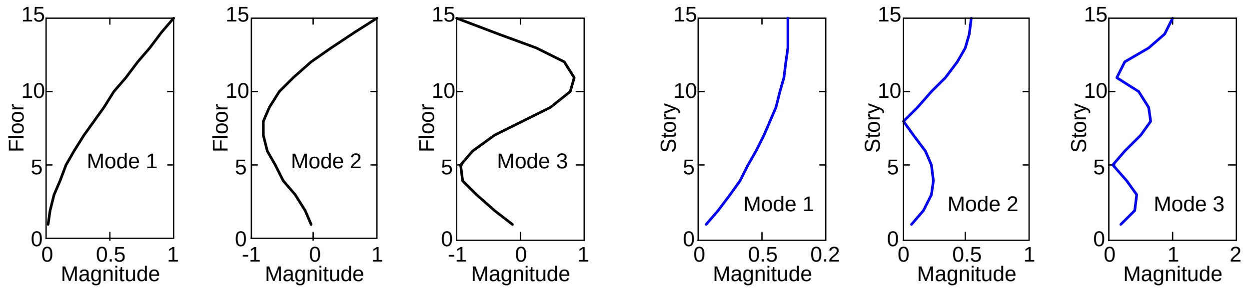

(b) Mode shapes of DBW

(c) Modal displacement demand of TVMDs

Fig. 6. Mode shape of DBW and modal displacement demand of TVMDs.

The mass ratio is an important parameter in the tuning design. In this study, the mass ratio μ_i for the TVMD coupled wall is defined as the ratio of the ith modal apparent mass of the TVMDs to the ith modal mass of the primary structure, given by [27]:

$$\mu_i = \frac{\{\phi_{di}\}^{\mathrm{T}}[\mathrm{M_r}]\{\phi_{di}\}}{\{\phi_i\}^{\mathrm{T}}[M_{\mathrm{p}}]\{\phi_i\}} \tag{8}$$

where $\{\phi_i\}$ and $\{\phi_{di}\}$ denote the ith real mode shape vector of the primary structure (i.e., the DBW) and the correponding modal displacement demand vector of TVMDs, $[M_{\mathrm{p}}]$ denotes the mass matrix of the primary structure, and the matric $[M_{\mathrm{r}}]$ is defined by Eq. (9).

$$[M_{\mathrm{r}}]=\begin{bmatrix} m_{\mathrm{r}1} & 0 & \cdots & 0 \\ 0 & m_{\mathrm{r}2} & \cdots & 0 \\ \vdots & \vdots & \ddots & \vdots \\ 0 & 0 & \cdots & m_{\mathrm{r}n} \end{bmatrix} \tag{9}$$

In the matric, the jth diagonal term $m_{\mathrm{r}j}$ denotes the apparent mass of TVMD in the jth story.

The single-mode tuning design procedure is as follows. *(1) Calculate the modal properties of the primary structure and select the target tuning mode.* *(2) Determine the apparent masses of TVMDs.* For a selected tuning mode and a given mass ratio of μ_i, the apparent mass vector of TVMDs $\{m_{\mathrm{r}1}, m_{\mathrm{r}2}, \ldots, m_{\mathrm{r}n}\}^{\mathrm{T}}$ can be calculated by assuming it to be proportional to $\{\phi_{\mathrm{d}i}\}$ and using Eqs. (8) and (9). *(3) Determine the optimal frequency and damping ratio of TVMDs.* For the target tuning modal frequency ω_i and a given mass ratio μ_i, the optimal frequency $\omega_{\mathrm{d}}^{opt}$ and optimal damping ratio $\varsigma_{\mathrm{d}}^{opt}$ of the TVMDs can be calculated by the fixed point method using Eqs. (6) and (7). *(4) Determine the stiffness and damping parameters for TVMDs.* The spring stiffness $k_{\mathrm{b}j}$ and damping coefficient of dashpot $c_{\mathrm{d}j}$ of the TVMD in the jth story are determined as follows

$$k_{\mathrm{bj}}=m_{\mathrm{rj}}\left(\omega_{\mathrm{d}}^{\mathrm{opt}}\right)^2 \tag{10}$$

$$c_{\mathrm{dj}}=2m_{\mathrm{rj}}\omega_{\mathrm{d}}^{\mathrm{opt}}\varsigma_{\mathrm{d}}^{\mathrm{opt}} \tag{11}$$

where the m_{rj} denotes the apparent mass of the TVMD in the jth story.

3.2. Dynamic properties of TCW

For the prototype DBW, if the mass ratio is set to $\mu_i = 0.6$, the parameters of the TVMDs can be determined using the above single-mode tuning method. Note that such a high mass ratio can be realized due to very large amplification effect of ball screw mechanism on the physical mass of TVMDs. Table 1 summarizes the optimal design parameters of TVMDs. The 2nd to 4th columns of this table are the results obtained from the aforementioned single mode tuning design method, where the target tuning mode is selected as the 1st, 2nd and 3rd mode of the DBW, respectively. The last column of Table 1 is the results obtained from the multi-mode tuning design method, which will be presented in the following Section 4.

Table 1. Optimal design parameters for TVMDs.

	Tuned to 1st mode			Tuned to 2nd mode			Tuned to 3rd mode			Multi-mode tuning (group scenario 1-2-3)		
Story	m_r (ton)	k_b (kN/mm)	c_d (kNs/mm)	m_r (ton)	k_b (kN/mm)	c_d (kNs/mm)	m_r (ton)	k_b (kN/mm)	c_d (kNs/mm)	m_r (ton)	k_b (kN/mm)	c_d (kNs/mm)
1	100	1.9	0.50	27	17.6	0.78	19	85.0	1.4	78	0.46	0.34
2	290	5.5	1.4	71	45.9	2.0	44	195.3	3.2	78	0.46	0.34
3	461	8.8	2.3	96	62.4	2.8	47	208.3	3.4	78	0.46	0.34
4	614	11.7	3.0	104	67.7	3.0	32	141.1	2.3	78	0.46	0.34
5	749	14.3	3.7	97	62.9	2.8	5	22.1	0.36	78	0.46	0.34
6	873	16.6	4.3	74	48.0	2.1	28	121.3	2.0	110	134.0	2.1
7	986	18.8	4.9	38	24.9	1.1	57	248.7	4.1	110	134.0	2.1
8	1081	20.6	5.3	5	3.3	0.15	72	316.0	5.2	110	134.0	2.1
9	1156	22.0	5.7	52	33.7	1.5	70	306.1	5.0	110	134.0	2.1
10	1216	23.2	6.0	98	63.6	2.8	50	219.6	3.6	110	134.0	2.1
11	1263	24.1	6.2	142	92.4	4.1	15	64.6	1.1	161	900.0	7.5
12	1299	24.7	6.4	181	117.8	5.2	29	126.2	2.1	161	900.0	7.5
13	1321	25.2	6.5	209	136.0	6.1	68	299.8	4.9	161	900.0	7.5
14	1333	25.4	6.6	226	147.1	6.5	96	423.5	7.0	161	900.0	7.5
15	1337	25.5	6.6	234	151.6	6.7	110	482.9	7.9	161	900.0	7.5
Sum	14079	268.2	69.7	1656	1074.9	47.8	743	3260.7	53.5	1746	5172.1	49.7

Due to the addition of TVMDs, the TCW system is non-classically damped. Therefore, complex modal analysis is conducted to yield the complex modal properties of the system. The details of the complex modal analysis and the calculation of participation mode vectors for a MDOF system incorporated with TVMDs are described in Ikago et al. [24]. Table 2 summaries the dynamic properties of an example of the TCW where TVMDs are tuned to the 2nd mode of the primary structure. The participation mode vectors of this TCW are shown in Fig. 7, compared with those of the DBW. Note that the *i*th participation mode vector for the TCW is calculated from the *i*th conjugated pair of complex mode shape vectors, while that for the DBW is calculated from the *i*th real mode shape vector.

Table 2. Dynamic properties of the DBW and TCW tuned to 2nd mode.

DBW			TCW		
Mode	Period (s)	Damping ratio	Mode	Period (s)	Damping ratio
1	2.276	0.050	1	2.357	0.422
2	0.390	0.025	2	0.521	0.609
			3	0.290	0.599
			4	0.260	0.591
			5	0.254	0.583
			6	0.251	0.577
			7	0.249	0.573
			8	0.248	0.571
			9	0.248	0.570
			10	0.247	0.569
			11	0.247	0.568
			12	0.247	0.568
			13	0.247	0.568
			14	0.247	0.567
			15	0.247	0.567
			16	0.245	0.550
			17	0.198	0.237
3	0.144	0.050	18	0.119	0.062
4	0.074	0.093	19	0.069	0.086
5	0.046	0.147	20	0.044	0.141
$T_d^{opt}=2\pi/\omega_d^{opt}=0.247$ s; $\varsigma_d^{opt}=0.57$					

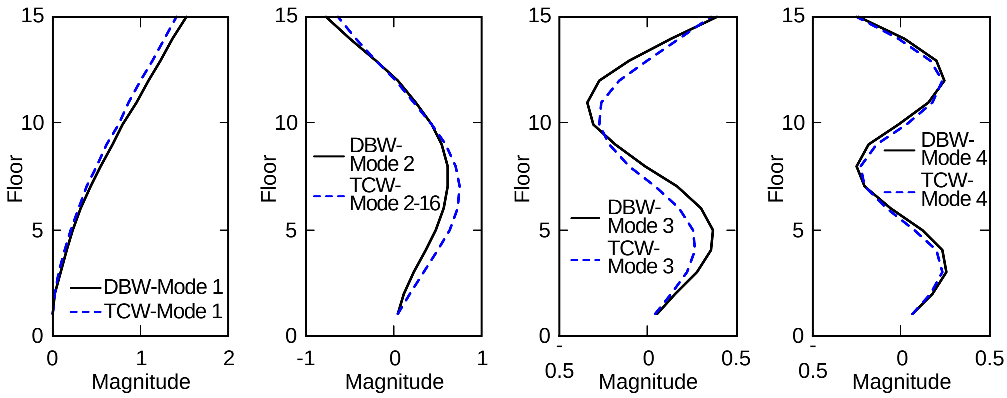

Fig. 7. Participation mode vectors of DBW and TCW tuned to the 2nd mode.

The following observations can be made from Table 2 and Fig. 7. (1) The target tuning mode (i.e., the 2nd mode of DBW) is split into 16 modes (i.e., the 2nd to 17th modes of the TCW system) due to addition of 15 TVMDs. Among these 16 modes, the first and the last modes are dominated by global vibration of the coupled wall system, while the others are the local vibration mode of TVMDs that have vibration periods and damping ratios close to those values of the TVMDs themselves (i.e., T_{d}^{opt} and $\varsigma_{\mathrm{d}}^{opt}$). (2) The combination of the 2nd to 17th participation mode vectors is nearly identical to the 2nd mode shape of the DBW. The 1st, 18th and 19th participation mode vectors correlate well with the 1st, 3rd and 4th participation mode vectors of the DBW. (3) The addition of TVMDs significantly increases the damping ratios for both the tuning mode (i.e., the 2nd mode) and the lower-order modes (e.g., the 1st mode) of the primary structure, while it has limited influence on damping properties of higher-order modes. Interestingly, this characteristic of damping supplied by TVMDs is different from either conventionally viscous dampers that provide damping for all modes or tuned mass damper (TMD) that absorb the vibration at a narrow frequency range of the tuning mode. The unique damping characteristic can be explained by dynamic analysis of TVMDs. As shown in Fig. 8, for a given TVMD excited by a sinusoid displacement load $u_t = U_t \sin(\omega t)$, the deformation of the dashpot u_{d} and that of the spring u_{k} can be obtained as detailed in Appendix. Fig. 8 shows the magnitude and phase angle of the responses of u_{d} and u_{k} relative to the excitation displacement u_{t}. When the excitation frequency ω_{L} is far lower than the natural frequency of TVMD ω_{n}, the viscous damper response dominates the total displacement ($U_{\mathrm{d}} / U_{\mathrm{t}} \approx 1$) while the spring has very limited deformation ($U_{\mathrm{k}} / U_{\mathrm{t}} \approx 0$), because the equivalent dynamic stiffness of viscous damper $c_{\mathrm{d}}\omega_{\mathrm{L}}$ is much lower than the stiffness of spring k_{b}. The cyclic responses of viscous damper with large magnitudes can thus dissipate energy and supply additional damping to the low-frequency vibration (e.g.., the lower-order mode). On contrast, when the excitation frequency ω_H is higher than the natural frequency of TVMD ω_n, the spring dominates the total displacement ($U_k / U_t \approx 1$) while the relative displacement of viscous damper is close to zero ($U_d / U_t \approx 0$). Very limited cyclic responses of viscous damper cannot provide substantial damping to high-frequency vibration (e.g., the higher-order mode). When the excitation frequency is close to ω_n, the TVMD resonates, accomplished by the opposite deformation of spring and viscous damper (i.e., the phase angle of spring and viscous damper displacement is approximately 180°, as shown in Fig. 8). Therefore, the motion of viscous damper is amplified ($U_d / U_t > 1$), leading to an increased damping supplement to the tuning mode.

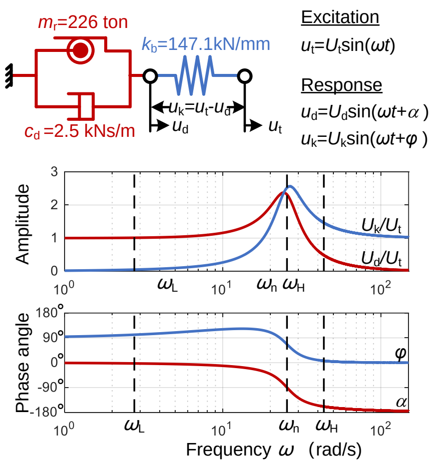

Fig. 8 Dynamic responses of TVMD under sinusoid excitation

Fig. 9 shows transfer functions from the base acceleration excitation to the top lateral displacement and acceleration responses for both the DBW and TCW systems. Note that the transfer functions are calculated in Matlab from state-space functions of the systems. Three models are considered for the TVMD coupled wall systems, i.e., TCW-1st, TCW-2nd and TCW-3rd, where the TVMDs are tuned to the first, second and third mode, respectively. The lateral displacement is dominated by the first mode whereas the acceleration response has significant contributions from all first three modes. Therefore, effective control of the acceleration response of high-rise buildings should act to suppress the vibration of a few modes. Furthermore, it can be observed from the figure that the addition of TVMDs can reduce the peak values of transfer function at both the frequency of the tuning mode and at the frequencies of lower-order modes. Therefore, TVMDs tuned to the 2nd or 3rd mode appears to be more efficient than those tuned to the 1st mode in terms of response control, particularly for the acceleration control.

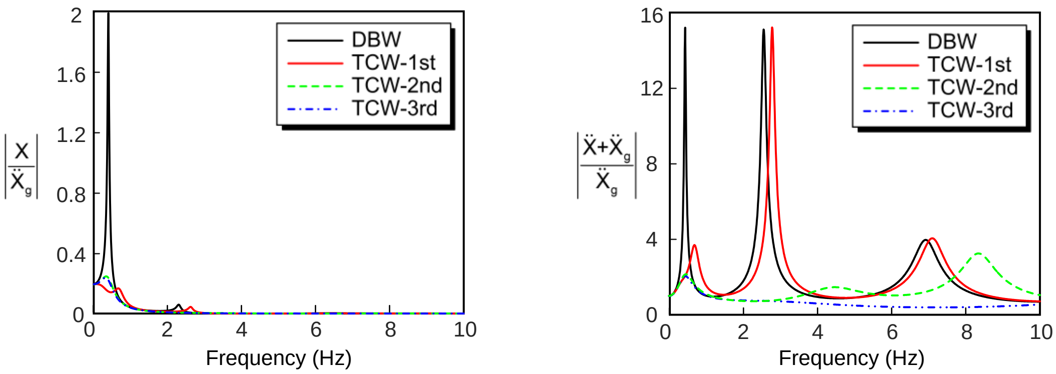

(a) Top displacement transfer function (b) Top acceleration transfer function

Fig. 9. Transfer function of DBW and TCW designed by single-mode tuning method.

3.3. Seismic response analysis

Seven ground motions are selected from NGA West 2 Ground Motion Database [38] using the linear scaling method such that the mean square error (MSE) of their acceleration response spectra is minimized with respect to the target spectrum over the period range of interest. The target spectrum for record selection is the DBE response spectrum specified in Chinese code for seismic design of buildings GB 50011-2010 [34]. The period range of interest is selected to span [0.1 s, T_g] and [T_g-0.2 s, 2T_g], where T_g denotes the characteristic site period [5]. In selecting the ground motions, record characteristics with magnitudes greater than 6, average shear wave velocity consistent with Site Class III and no restriction on fault type and fault distance were used as search criteria. Fig. 10 plots the time history of the selected seven ground motion records, the individual record spectra, the mean spectrum of the selected records and the target spectrum.

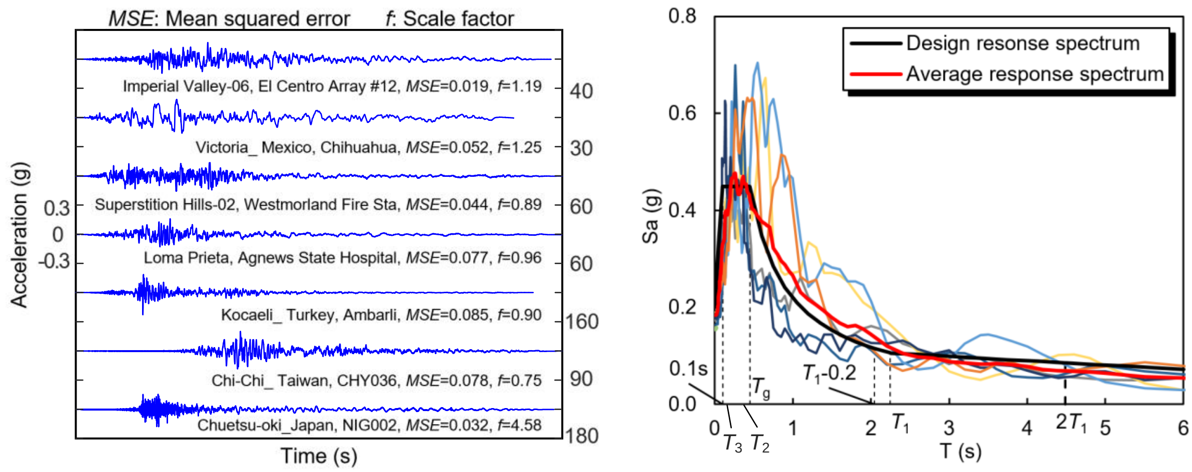

(a) Acceleration time history (b) Response spectra

Fig. 10. Time-history records and spectra of selected ground motions.

In this study, linear time-history analysis using a simplified numerical model developed in Subsection 2.4 is conducted to validate the effectiveness of the TVMD coupled wall system. Development of sophisticated nonlinear model of TVMD coupled wall system, which can reflect the nonlinearity in TVMDs and elastic-to-plastic behavior of walls piers, is out of the scope of this paper. Fig. 11 shows the mean values of the maximum inter-story drifts and floor accelerations at each floor of the DBW and TCW when subjected to the seven ground motions. The maximum inter-story drift of the TCW-1st is up to 51% lower than the DBW, while the maximum floor acceleration of both systems is similar. This is because TVMDs tuned to the 1st mode cannot suppress the higher-mode vibrations, while they significantly contribute to floor accelerations as can be observed from the shape of acceleration distribution of the DBW (see Fig. 11). The TCW-2nd and TCW-3rd demonstrate nearly identical responses in terms of both the inter-story drifts and floor accelerations. Both models decrease the inter-story drifts and floor accelerations by approximately 60% and 65% respectively, compared with the DBW.

The analysis also indicates that the sum of the maximum absolute values of forces for all TVMDs (referred to as “the total TVMD force” hereinafter) is 3270 kN, 2460 kN and 2500 kN for TCW-1st, TCW-2nd and TCW-3rd, respectively. Therefore, TVMDs tuned to the 2nd or 3rd modes do not necessarily require larger force capacity than those tuned to the 1st mode, although the former shows superior performance. As such, allowing for controlling both inter-story drifts and floor accelerations, design of TVMDs tuned to at least the second mode of the primary structure is recommended for the TVMD coupled wall system. Note that the maximum force of a TVMD is calculated as 456 kN under the DBE motions. A pair of TVMDs connected to one joint result in a maximum vertical shear force demand of 570 kN to the joint, while the horizontal force demand to the joint is quite small because the horizontal force components of two TVMDs can partially counter-act each other. For a conventional coupled wall system, the beam-to-wall joint are easily design to have a capacity to resist the vertical shear force with a magnitude of 1000 kN induced by the coupling beam. Therefore, the local region of the wall piers at the TVMD-to-wall joints would not sustain damage in such force demands, except for the joint at the top floor that connects only to one TVMD and may sustain large horizontal tensile force demand.

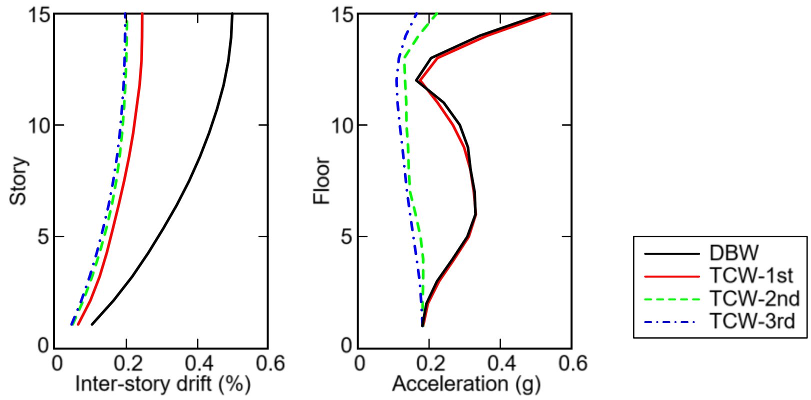

(a) Inter-story drifts (b) Floor accelerations

Fig. 11. Seismic responses (single-tuning method results).

It should be noted that the above analysis results are for the TVMD coupled walls designed with an apparent mass ratio of 0.6. One might be interested in how the apparent mass ratio influences the results. In fact, an increase of apparent mass ratio leads to an increased force of the TVMDs, while the economic cost of TVMDs is almost proportional to their force capacity. Additional analysis was conducted, where the TVMDs were tuned to the 3rd mode while the mass ratio was taken as a variable, ranging from zero to 0.6. For each mass ratio value, the TVMD parameters were determined by the single-tuning design procedure, and then the history response analysis was conducted to obtain the responses of the TCW and TVMD forces when subjected to the selected seven ground motions. Fig. 12 plots the relation of the mean values of the maximum top lateral displacement (or the maximum top floor acceleration) versus the total TVMD force. It is observed that the maximum lateral displacement is approximately inversely proportional to the total TVMD force. The maximum top floor acceleration decreases rapidly along with an increase of the total TVMD force upon to 2500 kN, while it remains stable as approximately 0.2 g for further increase of TVMD forces. Therefore, a reasonable apparent mass ratio should be chosen for TVMD coupled wall design, which would be determined through a consideration of required seismic control performance, economic costs and other engineering issues.

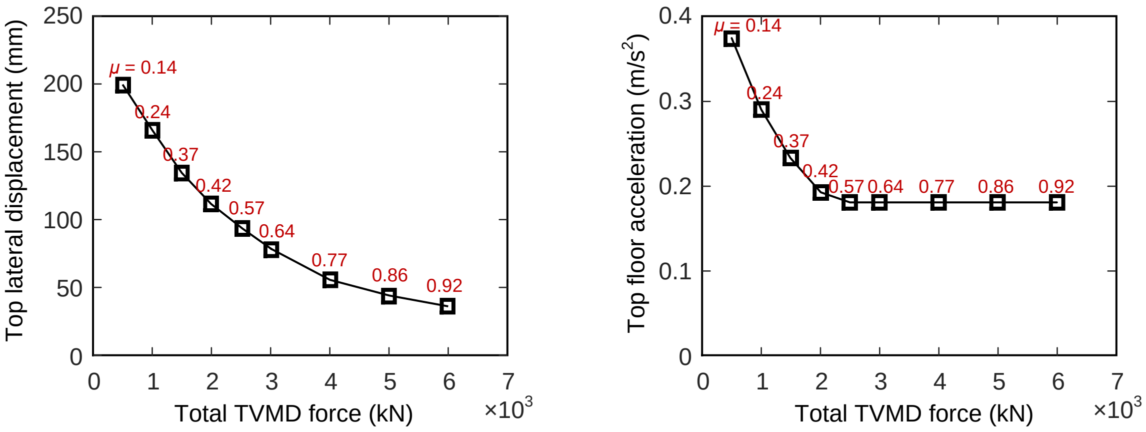

(a) Top lateral displacement (b) Top floor acceleration

Fig. 12. Seismic responses versus the total TVMD force at various mass ratio.

4. Multi-mode tuning design method

As a number of TVMDs are installed in the TVMD coupled wall system, one might naturally suggest developing a multi-mode optimal tuning design method in which different groups of TVMDs are tuned to different modes of the primary structure. In fact, the multi-mode tuning design concept has been applied to multi-story shear-type structures incorporated with TVMDs, where the numerical optimization is used to determine the parameters of TVMDs [23,27,28]. Similarly, in this paper the multi-mode tuning design of the TVMD coupled wall system is defined as an optimization problem as well.

In this optimization problem, the objective function is the sum of the normalized maximum inter-story drift and the normalized maximum floor acceleration, as presented in Table 3. The weight factor w in the objective function is taken as 0.5 in this study. $\bar{\theta}_{\max}$ and $\bar{a}_{\max}$ denote the mean value of the maximum inter-story drift and maximum floor acceleration of the structure when subjected to the seven selected motions shown in Fig.10. θ_s and a_s are taken as 1/450 (inter-story drift) and 0.2 g (i.e., PGA of DBE motions), respectively. Note that under the seven motions of DBE level, the maximum inter-story drift ratio for the TCW system designed by the single-mode tuning method varies among 1/500 to 1/400. Therefore, the average value of 1/450 is adopted as θ_s to normalize the inter-story drift responses.

In practice, the dampers installed in the buildings are usually grouped into a few capacity types, for ease of design, manufacture and installation. In this study, the fifteen TVMDs are divided into three groups; TVMD Type 1 installed for the 1st to 5th stories, TVMD Type 2 for the 6th to 10th stories, and TVMD Type 3 for the 11th to 15th stories. $(M_{r1}, w_{d1}, \varsigma_{d1})$, $(M_{r2}, w_{d2}, \varsigma_{d2})$, $(M_{r3}, w_{d3}, \varsigma_{d3})$ represent the apparent mass, natural frequency and damping ratio for the TVMDs of Type 1 through Type 3, respectively. These parameters are taken as the variables of the optimization problem. Because the economic cost of the TVMDs relates to their force capacity, the total TVMD force (i.e., the sum of the maximum absolute values of forces for all TVMDs $\sum F_{\max,j}$) is adopted as the constraint in this optimization. As the total TVMD force is approximately 2500 kN for the TCW-2nd and TCW-3rd in the previous section, $\sum F_{\max,j} \le 2500\text{kN}$ is used as the constraint for fair comparison between multi-mode tuning design and single-mode tuning design.

Table 3. Multi-mode tuning optimization problem.

Objective:	$\min\left[w\dfrac{\bar{\theta}_{\max}}{\theta_s} + (1-w)\dfrac{\bar{a}_{\max}}{a_s} \right]$	(w=0.5)
Variables:	$x = \begin{Bmatrix} M_{r1}, M_{r2}, M_{r3} \\ w_{d1},\ w_{d2},\ w_{d3} \\ \varsigma_{d1},\ \varsigma_{d2},\ \varsigma_{d3} \end{Bmatrix}^T$	
Constraints:	$\sum F_{\max,j} \le 2500\text{kN}$	

The sequential quadratic programming (SQP) method [39] is regarded as one of the most efficient methods to solve the constrained nonlinear optimization problem, and it has been successfully applied to optimization of TVMDs in shear-type structures [23,27]. Therefore, the SQP method is adopted in the following optimization procedure. The optimization results of the SQP method rely on the initial values of the variables. A total of six tuning group scenarios are considered as shown in Table 4, which correspond to six sets of initial values of the variables. For each scenario, after setting the initial values of apparent masses (M_{r1}, M_{r2} and M_{r3}), initial values of frequency (w_{d1}, w_{d2}, w_{d3}) and damping ratio $(\varsigma_{d1}, \varsigma_{d2}, \varsigma_{d3})$ are determined by the fixed point method, using Eqs. (6) and (7) by substituting the different tuning-mode frequencies of the primary structures. For example, the tuning group scenario “2-1-3” in Table 4 denotes that the initial values of TVMD parameters in the lower five stories (i.e., 1-5 stories) are determined by tuning the 2nd mode of the primary structure, those of the middle five stories (i.e., 6-10 stories) are determined by tuning the 1st mode, and those of the top five stories (i.e., 11-15 stories) are determined by tuning the 3rd mode. Afterwards, the optimization is conducted iteratively by using the time-history analysis and SQP algorithm.

Table 4. Tuning group scenarios of TVMDs.

Story	1st-5th stories	6th-10th stories	11th-15th stories	Tuning group scenario
Tuning Mode	1st	2nd	3rd	1-2-3
	1st	3rd	2nd	1-3-2
	2nd	1st	3rd	2-1-3
	2nd	3rd	1st	2-3-1
	3rd	1st	2nd	3-1-2
	3rd	2nd	1st	3-2-1

Fig. 13 shows the optimization results of multi-mode tuning for the TVMD coupled wall system. It appears that the group tuning scenario 1-2-3 and scenario 3-1-2 demonstrate the best performance. Table 1 lists the parameters for TVMDs obtained from the optimization design based on the tuning group scenario 1-2-3.

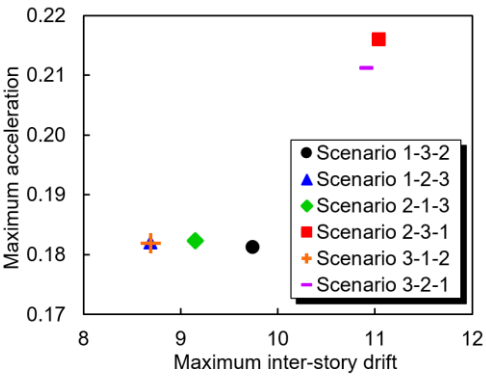

Fig. 13. Optimization results of multi-mode tuning design.

Fig. 14(a) and (b) show the transfer functions from the base acceleration excitation to the top lateral displacement and floor acceleration for the TCW-SQP system that is designed based on the optimization of the tuning group scenario 1-2-3. The transfer functions of the DBW and the TCWs designed using the single-mode tuning method are also plotted in the figure for comparison. TCW-SQP shows better performance for reducing the peak values of transfer functions as compared to the DBW system and TCW-1st model, while it shows very similar transfer functions to the TVW-3rd model.

Fig. 14(c) shows the mean values of the maximum inter-story drifts and floor accelerations of the TCW-SQP when subjected to the seven motions. Again, the TCW-SQP had much smaller responses than DBW and the TCW-1st model, while its responses are similar to those of TCW-2nd and TCW-3rd except for a slight difference in the floor accelerations. Fig. 14(d) and (e) plot the time histories of the top lateral displacement and top floor acceleration responses of the systems subjected to the Imperial Valley-06 motion. It is indicated that the TCW-1st leads to decreased displacement responses by suppressing the first mode vibration of the primary structure, while the TCW-2nd, TCW-3rd and TCW-SQP can further reduce the acceleration responses by suppressing higher-mode vibration. It may be recalled from Section 3, that the TVMDs tuned to a high-order mode can also provide large additional damping to the lower-order modes. Therefore, for the TVMD coupled wall system, the single-tuning design method is recommended using the 2nd or 3rd mode as the target tuning mode, since it can perform as well as the more complicated multi-mode tuning method.

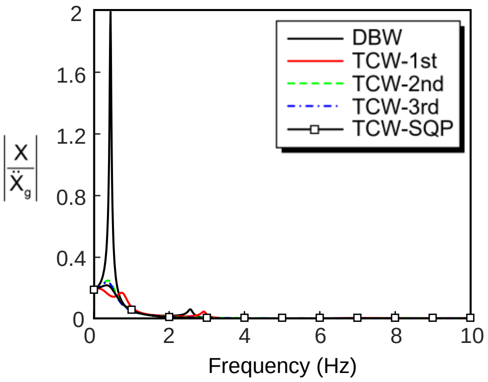

(a) Top displacement transfer function

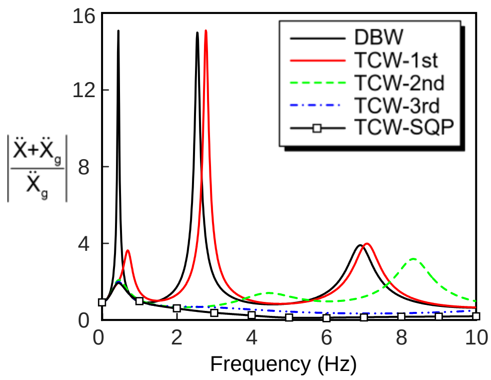

(b) Top acceleration transfer function

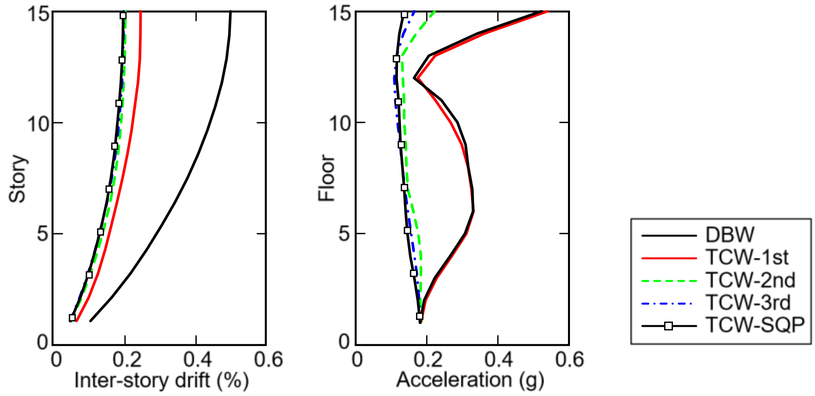

(c) Seismic responses of inter-story drift and floor acceleration

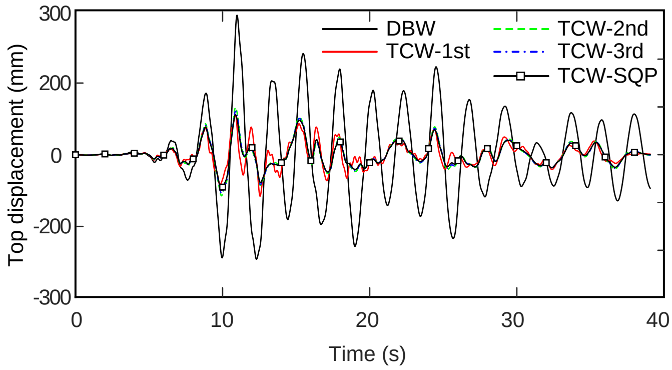

(d) Time history of top lateral displacement under the Imperial Valley-06 motion

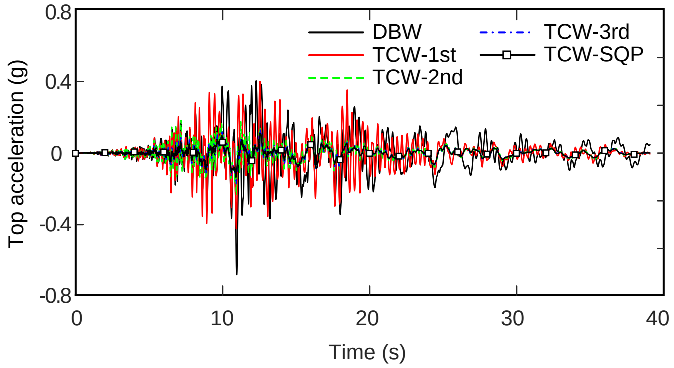

(e) Time history of top floor acceleration under the Imperial Valley-06 motion

Fig. 14. Responses of TCW designed by the multi-mode tuning method.

5. Real-time hybrid simulation (RTHS) of TCW system

RTHS [40,41] was conducted to examine the seismic performance of the TCW system. In this simulation, a viscous-mass damper was tested in the physical domain, while other structural components and dampers of the system were simulated in the numerical domain. Note that the objective of RTHS in this paper is to demonstrate the advantages of the TCW system. Therefore, only the TVMD in the top story that has the largest displacement and velocity was selected to test physically, and the nonlinearity of wall piers were simulated in simplified equivalent elastic model. Large-scale dynamic tests of the TCW system are necessary for examination its seismic performance, which would be a future research work.

5.1. Sub-TCW model and TVMD specimen

The TCW system designed using the multi-mode tuning method as described in Section 4 was considered as the prototype structure for the RTHS. Because only one TVMD is connected in the joint at the top floor (see Fig. 3), the forces of the TVMD may lead to large horizontal tensile force demand to the joint. In order to prevent the failure of the joint, the TVMD at the top story was redesigned by decreasing its damping coefficient, while its apparent mass and stiffness remained unchanged. Although this modification decreased the maximum force of the top-story TVMD applied to the joint, it affected slightly the dynamic response of the system, with an 8% increase in the maximum inter-story drift and nearly no change in the maximum floor acceleration.

As shown in Fig. 15, the TVMD in the top story was tested in the physical domain, the rest of the system was simulated in the numerical domain using a Sub-TCW model developed in Matlab. The experimental testing of the TVMD included only a rotary viscous mass damper, while the stiffness of the spring remained in the numerical model. To accommodate the loading capacity of the dynamic actuator, the apparent mass, damping coefficient and the corresponding force of the viscous mass damper was scaled down with a factor of 1/383. The parameters of the rotary viscous mass damper are summarized in Table 5. The flow diagram of RTHS for the TCW system is shown in Fig. 15. The RTHS was conducted with a very small time interval of 1/2000 second, to ensure the stability of integration.

Table 5. Parameters of TVMD specimen.

Flywheel mass m_f (kg)	Apparent mass m_r (kg)	Amplification factor m_r/m_f	Viscosity of viscous material (mm^2/s)	Damping coefficient c_d (kNs/m)	Frequency ω_d (rad/s)	Damping ratio ς_d
3.35	420	125	8000	2	74.8	0.03

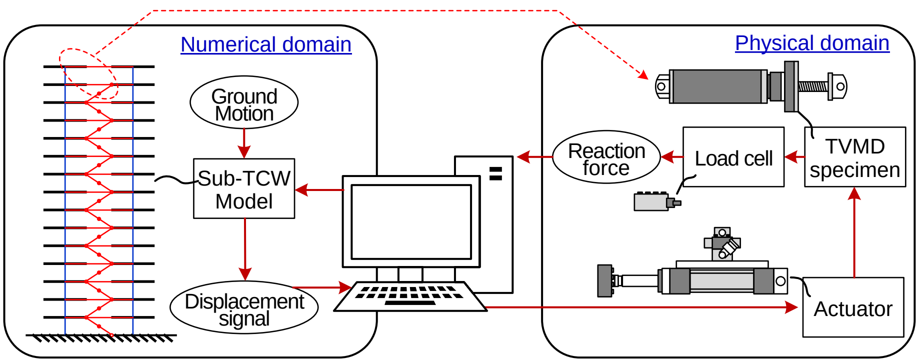

Fig. 15. Flow diagram of RTHS for TCW system.

5.2. Test setup and loading

Fig. 16 shows the schematic drawing and photograph of the test setup. The numerical model Sub-TCW was compiled in Simulink first and then downloaded to a dSPACE digital signal processing board. A system that uses proprietary software ControlDesk and Real-Time Interface (RTI) was adopted for digital signal control, information interaction and rapid iteration.

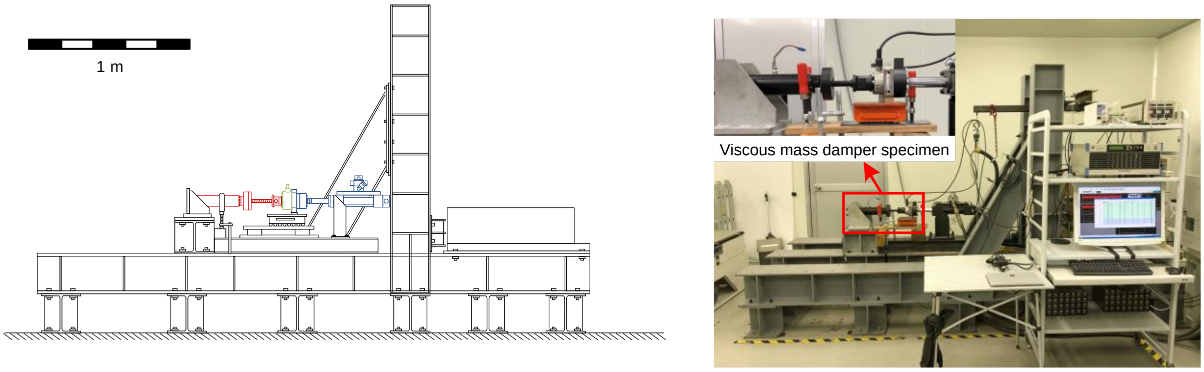

(a) Schematic drawing (b) Photograph

Fig. 16. Schematic drawing and photograph of test setup.

Three ground motions were selected as the input of the RTHS, and the time-history records scaled to the DBE level and the corresponding acceleration response spectra of the motions are shown in Fig. 17. One is the Imperial Valley-06 motion, recorded in the 1979 El Centro Earthquake, for which the acceleration response spectra matched well with the design response spectra. The others are the JMA Kobe motion, a near-field motion recorded in the 1995 Kobe earthquake and the Sakishima motion, a far-field motion recorded during the 2011 Tohoku-Oki earthquake. Note that the Sakishima motion is a long-period long-duration motion, and only a 120-second record with large-magnitude shaking was considered in this RTHS.

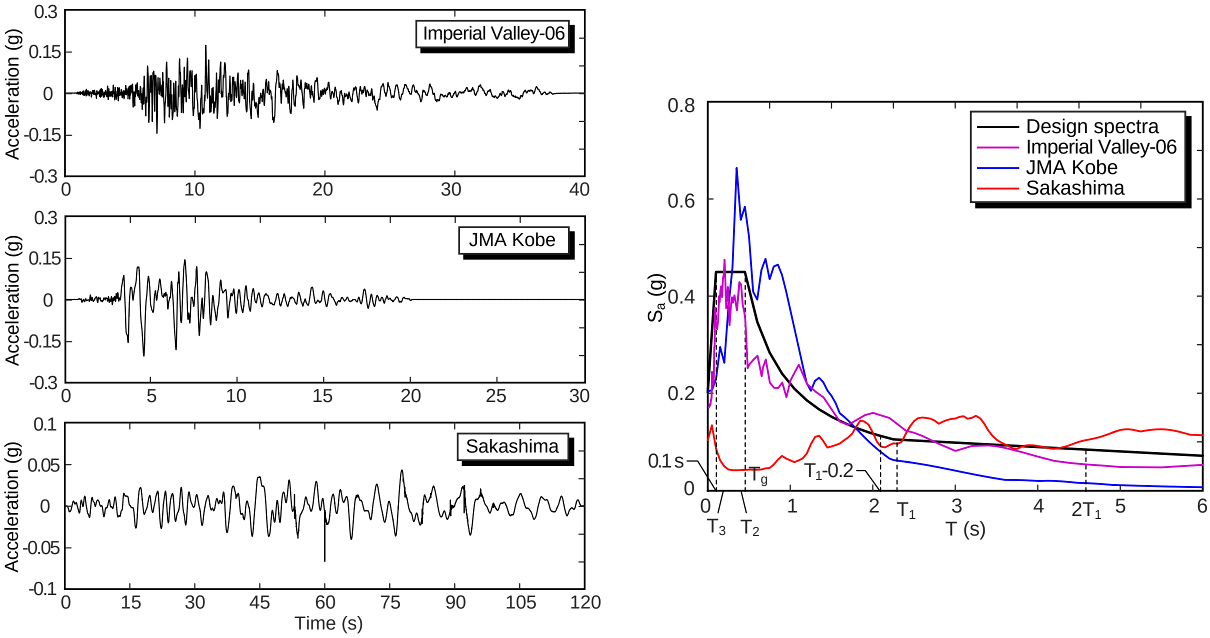

(a) Time-history records (b) Acceleration response spectra

Fig. 17. Time-history records and spectra of input motions.

Six load cases were considered for the RTHS, as listed in in Table 6. The Imperial Valley-06 motion was scaled into three levels: the SLE, DBE and the maximum considered earthquake (MCE). For the JMA Kobe and Sakishima motions, only the DBE level was considered. Because the predicted drifts of TCW system under DBE motions are rather small (with the maximum inter-story drift less than 0.25%), it is reasonable to simulate the wall piers using an elastic model. However, when subjected to the MCE motions, the wall piers undergo nonlinearity. Cracking of concrete and yielding of rebar would lead to decrease of the stiffness of walls and increase of damping of the primary structure. Particularly, the stiffness reduction results in elongation of the vibration periods of the system, and it may lead to the possible detuning effect as the structural vibration frequency shifts from the tuning frequency. In Case 6, an equivalent linear model was used to represent the nonlinearity, where the effective flexural stiffness of the RC walls in the first two stories (plastic-hinge region) was taken as 35% of the initial stiffness value E_cI_g based on the gross section properties, and the effective flexural stiffness of walls in other stories was taken as 70% of the stiffness value E_cI_g [42]. As the damping ratio of RC structure at yield point is recommended as 7% - 10% [43], an inherent damping ratio of 7% for the structure was adopted in Case 6. Note that, in Case 3, the elastic model of wall piers was intendedly used even for the MCE shaking. The comparison between Case 3 and Case 6 can quantify the influence of detuning effect on TCW system.

Table 6. Loading cases and results of RTHS.

Case no.	Ground motion	Seismic level	Maximum inter-story drift (%)	Maximum floor acceleration (g)	Note
1	Imperial Valley-06	SLE	0.075	0.052	
2	Imperial Valley-06	DBE	0.21	0.15	
3	Imperial Valley-06	MCE	0.42	0.30	
4	JMA Kobe	DBE	0.13	0.15	
5	Sakishima	DBE	0.21	0.07	
6	Imperial Valley-06	MCE	0.46	0.22	Consider wall stiffness reduction

5.3. Results of RTHS

Table 6 presents the results from the RTHS. A comparison of the results between Cases 4 and 5 indicates that the Sakishima motion (far-field motion) generates relatively larger inter-story drifts while the JMA Kobe motion (near-field motion) generates relatively larger floor accelerations. It is because the Sakishima motion consists of large low-frequency components that effectively excite the fundamental mode, while the JMA Kobe motion has the high-frequency components that stimulate the vibration of high modes. Further analysis indicates that, when subjected to the three motions under DBE level, the average values of the maximum inter-story drift and the maximum floor acceleration of TCW obtained from the RTHS are 64% and 76% lower than the responses of DBW obtained from numerical simulation. Therefore, the TCW system exhibits superior performance in controlling the dynamic responses of the structures, when subjected to various types of seismic motions.

Fig. 18 plots the time history response of the axial force of the viscous mass damper obtained from RTHS for Case 3, compared with the numerical analysis results. The difference between experimental test and analysis results majorly comes from the friction forces in the ball screw device, which is not considered in the numerical model of TVMDs. If including the friction forces measured from static tests of the ball screw device, the numerical model can generally track the response obtained from the RTHS, as indicated in Fig. 18.

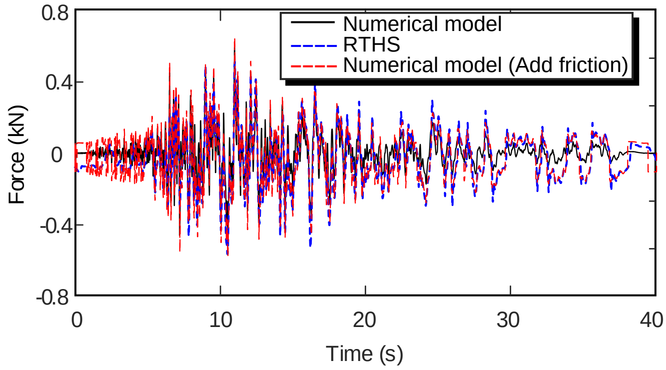

Fig. 18. Time history response of viscous mass damper force.

5.4. Detuning effect

Fig. 19 compares the results of Case 3 versus Case 6. Both cases had an identical ground motion, while the latter had reduced stiffness of the walls and increased structural damping ratio to simulate the effect of structural damage. The responses of the DBW obtained from the numerical analyses are also plotted in this figure. It is indicated that the decreased stiffness of the walls leads to an obvious increase in the inter-story drift and decrease in the floor acceleration of the DBW system. However, the responses of TCW system appear to be less sensitive to the decrease in the stiffness of the walls.

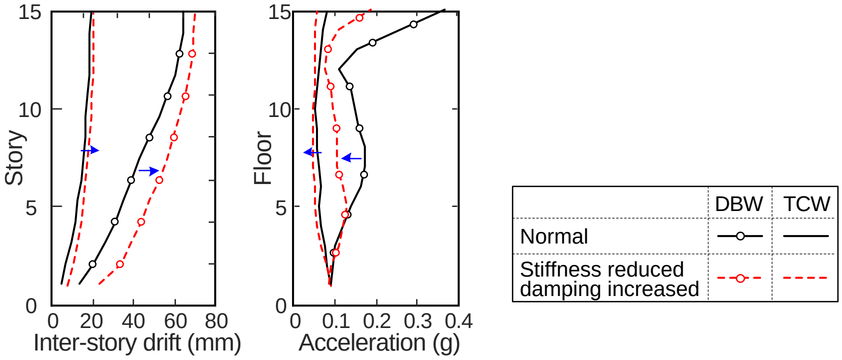

Fig. 19. Response comparison of Case 3 versus Case 6.

Past studies have demonstrated that, for the TMD system, the detuning effect (i.e., the deviation of the structure frequency from the tuning frequency) has an adverse influence on the structural dynamic response and leads to decrease in the efficiency of the TMD when subjected to strong motions [44]. However, the detuning effect appears to be limited for the TVMD coupled wall system. As shown in Fig. 19, the decrease of the stiffness of structural walls leads to only 9% increase in the inter-story drifts, and has almost no influence on the floor accelerations. A TMD is mobilized by the acceleration of the installation floor, and the floor acceleration, if its vibration frequency is shifted away from the TMD frequency, cannot effectively actuate the TMD oscillation. However, the TVMD is actuated by the relative movement at its two ends, and thus it is always mobilized if the structure undergoes the lateral vibration. In addition, a TVMD not only suppresses the dynamic response of the tuning mode, but can also provide additional damping to the vibration of which the frequencies are lower than the tuning frequency (as indicated in Fig. 9). Therefore, when the structure undergoes nonlinearity and its vibration frequency of the target tuning mode decreases, the TVMD still can suppress the vibration of that mode by providing additional damping.

6. Conclusions

This paper proposed an innovative TVMD coupled wall system for enhanced seismic performance of high-rise buildings. Both the simple-mode tuning method and multi-mode tuning method were developed for the optimal design of this system. Numerical analyses and real-time hybrid simulation (RTHS) were conducted to demonstrate the advantages of the proposed system, in terms of control of inter-story drifts and floor accelerations. The following conclusions are drawn from this study.

1) When designed using the proposed single-mode tuning method, the additional TVMDs can not only suppress the dynamic response of the tuning mode, but also provide additional damping to the lower-order modes.
2) Although the multi-mode tuning method based on SQP numerical optimization can control the dynamic responses of several modes simultaneously, the analysis indicates that it does not significantly improve upon the efficiency of the single-mode tuning method for TVMDs tuned to the 2nd or 3rd mode of the primary structure. Considering the simplicity of the procedure, the proposed single-mode tuning method is recommended.
3) The numerical analysis results indicate that, use of the TVMD coupled wall system can reduce both inter-story drifts and floor accelerations of a prototype 15-story building structure by approximately 60% and 65% respectively, compared to the isolated wall counterpart.
4) The real-time hybrid simulation (RTHS) further validates the effectiveness of the new system in seismic response control for high-rise buildings. Furthermore, the RTHS indicates that the detuning effect is slight for the TVMD coupled wall system even subjected to strong ground motions, due to the inherent advantages of TVMDs.

This paper illustrated the benefit of the proposed TVMD coupled wall system. Further research work should be performed for full development of this system, including (1) to develop high-fidelity numerical model of this system, which can reflects the nonlinearity of TVMDs and wall piers; (2) to conduct large-scale dynamic tests for understanding dynamic properties and nonlinear seismic responses of the system; (3) to compare with the coupled wall systems equipped with other types of dampers.

Acknowledgements

The work presented in this paper was sponsored by the Beijing Natural Science Foundation (Grant No. JQ18029), Tsinghua University Initiative Scientific Research Program (Grant No. 2019Z02TUU) and the Scientific Research Fund of the Institute of Engineering Mechanics, China Earthquake Administration (Grant No. 2018C01). The authors wish to express their sincere gratitude to the sponsors. The authors would like to acknowledge Osaka Prefecture and Dr. Toshihide Kashima of the Building Research Institute of Japan for providing the Sakishima site record of the 2011 Tohoku-Oki Earthquake.

Appendix

For a TVMD as shown in Fig. 8, the force equilibrium and deformation compatibility yield the following equations

$$m_{\mathrm{r}}\ddot{u}_{\mathrm{d}} + c_{\mathrm{d}}\dot{u}_{\mathrm{d}} = k_{\mathrm{b}}u_{\mathrm{k}} \tag{A1}$$

$$u_{\mathrm{k}} + u_{\mathrm{d}} = u_{\mathrm{t}} \tag{A2}$$

where the m_{r}, c_{d} and k_{b} denote the apparent mass of inerter, viscous coefficient of dashpot and stiffness of spring, respectively; u_{d} and u_{k} denote the dashpot deformation and spring deformation, respectively; and u_{t} denotes the displacement excitation on the TVMD.

Eqs. (A1) and (A2) yield the following equations of motions for a TVMD when subjected to displacement excitation of $u_{\mathrm{t}}(t)$

$$m_{\mathrm{r}}\ddot{u}_{\mathrm{d}} + c_{\mathrm{d}}\dot{u}_{\mathrm{d}} + k_{\mathrm{b}}u_{\mathrm{d}} = k_{\mathrm{b}}u_{\mathrm{t}} \tag{A3}$$

$$m_{\mathrm{r}}\ddot{u}_{\mathrm{k}} + c_{\mathrm{d}}\dot{u}_{\mathrm{k}} + k_{\mathrm{b}}u_{\mathrm{k}} = m_{\mathrm{r}}\ddot{u}_{\mathrm{t}} + c_{\mathrm{d}}\dot{u}_{\mathrm{t}} \tag{A4}$$

For the sinusoid excitation $u_{\mathrm{t}} = U_{\mathrm{t}}\sin(\omega t)$, the dashpot deformation is assumed as $u_{\mathrm{d}} = U_{\mathrm{d}}\sin(\omega t + \alpha)$. Therefore, Eq. (A3) yields

$$\left(k_{\mathrm{b}} - m_{\mathrm{r}}\omega^2\right)U_{\mathrm{d}}\sin(\omega t + \alpha) + c_{\mathrm{d}}\omega U_{\mathrm{d}}\cos(\omega t + \alpha) = k_{\mathrm{b}}U_{\mathrm{t}}\sin(\omega t) \tag{A5}$$

where α denotes the phase angle between the response u_{d} and excitation u_{t}.

Eq. (A3) is simplified as

$$\sqrt{\left(k_{\mathrm{b}} - m_{\mathrm{r}}\omega^2\right)^2 + \left(c_{\mathrm{d}}\omega\right)^2}\,U_{\mathrm{d}}\sin(\omega t + \alpha + \beta) = k_{\mathrm{b}}U_{\mathrm{t}}\sin(\omega t) \tag{A6}$$

where $\beta = \tan^{-1}\left(\dfrac{c_{\mathrm{d}}\omega}{k_{\mathrm{b}} - m_{\mathrm{r}}\omega^2}\right), \left(\beta \in [0°, 180°]\right)$.

Based on Eq. (A6), the magnitude and phase angle of the transfer function from the excitation u_{t} to the dashpot response u_{d} are solved as follows

$$\frac{U_{\mathrm{d}}}{U_{\mathrm{t}}} = \frac{k_{\mathrm{b}}}{\sqrt{\left(k_{\mathrm{b}} - m_{\mathrm{r}}\omega^2\right)^2 + \left(c_{\mathrm{d}}\omega\right)^2}} \tag{A7}$$

$$\alpha = -\beta = -\tan^{-1}\left(\frac{c_{\mathrm{d}}\omega}{k_{\mathrm{b}} - m_{\mathrm{r}}\omega^2}\right), \left(\alpha \in [-180°, 0°]\right) \tag{A8}$$

The natural frequency ω_{d} and damping ratio ς_{d} of TVMD are defines as

$$\omega_{\mathrm{n}} = \sqrt{k_{\mathrm{b}} / m_{\mathrm{r}}} \tag{A9}$$

$$\varsigma = c_{\mathrm{d}} / 2m_{\mathrm{r}}\omega_{\mathrm{n}} \tag{A10}$$

By substituting the frequency ratio $\gamma = \omega / \omega_{\mathrm{d}}$ and Eqs. (A9) and (A10) into Eqs. (A7) and (A8), the transfer function can be reformulated as

$$\frac{U_{\mathrm{d}}}{U_{\mathrm{t}}}=\frac{1}{\sqrt{\left(1-\gamma^2\right)^2+\left(2\varsigma\gamma\right)^2}} \tag{A11}$$

$$\alpha=-\tan^{-1}\left(\frac{2\varsigma\gamma}{1-\gamma^2}\right),\left(\alpha\in\left[-180°,0°\right]\right) \tag{A12}$$

The deformation of spring is assumed as $u_{\mathrm{k}}=U_{\mathrm{k}}\sin\left(\omega t+\varphi\right)$, where φ denotes the phase angle between the excitation of u_{t} and response u_{k}. Similarly, based on Eq. (4), the magnitude and phase angle of the transfer function from the excitation u_{t} to the spring response u_{k} are given by

$$\frac{U_{\mathrm{k}}}{U_{\mathrm{t}}}=\sqrt{\frac{\gamma^4+\left(2\varsigma\gamma\right)^2}{\left(1-\gamma^2\right)^2+\left(2\varsigma\gamma\right)^2}}, \tag{A13}$$

$$\varphi=\tan^{-1}\left(\frac{2\varsigma\gamma}{\left(2\varsigma\gamma\right)^2-\gamma^2\left(1-\gamma^2\right)}\right),\left(\varphi\in\left[0°,180°\right]\right). \tag{A14}$$

References

[1] Kam WY, Pampanin S, Elwood K. Seismic performance of reinforced concrete buildings in the 22 Feburary Christchurch (Lyttelton) earthquake. Bulletin of the New Zealand Society for Earthquake Engineering, 2011, 44(4): 239-78.

[2] Ji X, Kajiwara K, Nagae T, Enokita R, Nakashima M. A substructure shaking table test for reproduction of earthquake responses of high-rise buildings. Earthq Eng Struct Dyn 2009; 38(12):1381-99.

[3] Kasai K, Pu W, Wada A. Responses of tall buildings in Tokyo during the 2011 Great East Japan Earthquake. Proceedings of Behavior of Steel Structures in Seismic Areas (STESSA 2012), Santiago, Chile, 2012; 25-35.

[4] Ji X, Wang Y, Ma Q, Okazaki T. Cyclic behavior of replaceable steel coupling beams. J Struct Eng 2017; 143(2): 04016169.

[5] Ji X, Liu D, Sun Y, Molina Hutt C. Seismic performance assessment of a hybrid coupled wall system with replaceable steel coupling beams versus traditional RC coupling beams.

Earthq Eng Struct Dyn 2017; 46(4): 517-35.

[6] Ji X, Wang Y, Zhang J, Okazaki T. Seismic behavior and fragility curves of replaceable steel coupling beams with slabs. Eng Struct 2017; 150: 622-35.

[7] Qu Z, Ji X, Shi X, Wang Y, Liu H. Cyclic loading test of steel coupling beams with mid-span friction dampers and RC slabs. Eng Struct 2020; 203: 109876.

[8] Christopoulos C, Montgomery MS. Viscoelastic coupling dampers (VCDs) for enhanced wind and seismic performance of high-rise buildings. Earthq Eng Struct Dyn 2013; 42(15): 2217-33.

[9] Ji X, Liu D, Molina Hutt C. Seismic performance evaluation of a high-rise building with novel hybrid coupled walls. Eng Struct 2018; 169: 216-25.

[10] Saito K, Sugimura Y, Nakaminami S, Kida H, Inoue N. Vibration tests of 1-story response control system using inertial mass and optimized soft spring and viscous element. Proceedings of the 14th World Conference on Earthquake Engineering, Beijing, China, 2008; Paper No. 12-01-0128.

[11] Ikago K, Saito K, Inoue N. Seismic control of single-degree-of-freedom structure using tuned viscous mass damper. Earthq Eng Struct Dyn 2012; 41(3): 453-74.

[12] Smith MC. Synthesis of mechanical networks: the inerter. IEEE T Automat Contr 2002; 47(10): 1648-62.

[13] Papageorgiou C, Smith MC. Laboratory experimental testing of inerters. Proceedings of the 44th IEEE Conference on Decision and Control. Seville, Spain, 2005; 3351-3356.

[14] Wang FC, Hong MF, Lin TC. Designing and testing a hydraulic inerter. Proc Inst Mech Eng Part C J Mech Eng Sci. 2011; 225(1): 66-72.

[15] Swift SJ, Smith MC, Glover AR, Papageorgiou C, Gartner B, Houghton NE. Design and modelling of a fluid inerter. Int J Control. 2013; 86(11): 2035-2051.

[16] Zhu S, Shen W ai, Xu Y lin. Linear electromagnetic devices for vibration damping and energy harvesting: Modeling and testing. Eng Struct. 2012 ; 34:198-212.

[17] Gonzalez-Buelga A, Clare LR, Neild SA, Jiang JZ, Inman DJ. An electromagnetic inerter-based vibration suppression device. Smart Mater Struct. 2015; 24(5): 055015.

[18] Lazar IF, Neild SA, Wagg DJ. Using an inerter-based device for structural vibration suppression. Earthq Eng Struct Dyn 2014; 43(8): 1129-47.

[19] Marian L, Giaralis A. Optimal design of a novel tuned mass-damper-inerter (TMDI) passive vibration control configuration for stochastically support-excited structural systems. Probabilistic Eng Mech 2014; 38: 156-64.

[20] Lazar IF, Neild SA, Wagg DJ. Vibration suppression of cables using tuned inerter dampers. Eng Struct 2016; 122: 62-71.

[21] Sun L, Hong D, Chen L. Cables interconnected with tuned inerter damper for vibration mitigation. Eng Struct 2017; 151: 57-67.

[22] Ye K, Shu S, Hu L, Zhu H. Analytical solution of seismic response of base-isolated structure with supplemental inerter. Earthq Eng Struct Dyn 2019;48(9):1083-90.

[23] Ikago K, Saito K, Inoue N. Optimum multi-modal seismic control design of high-rise buildings using tuned viscous mass dampers. Proc. 13th Int. Conf. Civil, Struct. Environ. Eng. Comput., 2011; Paper No. 164.

[24] Ikago K, Sugimura Y, Saito K, Inoue N. Modal response characteristics of a multiple-degree-of-freedom structure incorporated with tuned viscous mass dampers. J Asian Archit Build 2012; 11(2): 375-82.

[25] Ikago K, Inoue N. Fundamental modes of seismic control multi-story shear building using tuned viscous mass damper: An analytical study on a case in which the secondary mass distribution is proportional to that of primary stiffness. Proceedings of 13th World Conference on Seismic Isolation, Energy Dissipation and Active Vibration Control of Structures, Sendai, Japan, 2013; Paper No. 900718.

[26] Marian L, Giaralis A. Optimal design of a novel tuned mass-damper-inerter (TMDI) passive vibration control configuration for stochastically support-excited structural systems.

Probabilistic Eng Mech 2014; 38: 156-64.

[27] Ikago K, Sugimura Y, Saito K, Inoue N. Optimum seismic response control of multiple degree of freedom structures using tuned mass viscous mass dampers. Proceedings of the 10th International Conference on Computational Structures Technology, Stirlingshire, Scotland, 2010; Paper No. 164.

[28] Wen Y, Chen Z, Hua X. Design and evaluation of tuned inerter-based dampers for the seismic control of MDOF structures. J Struct Eng 2016; 143(4): 04016207.

[29] Zhang SY, Jiang JZ, Neild S. Optimal configurations for a linear vibration suppression device in a multi-storey building. Struct Control Heal Monit 2017; 24: 1-17.

[30] Pan C, Zhang R, Luo H, Li C, Shen H. Demand-based optimal design of oscillator with parallel-layout viscous inerter damper. Struct Control Heal Monit 2018; 25: 1-15.

[31] Ruiz R, Taflanidis AA, Giaralis A, Lopez-Garcia D. Risk-informed optimization of the tuned mass-damper-inerter (TMDI) for the seismic protection of multi-storey building structures. Eng Struct 2018; 177: 836-50.

[32] Taflanidis AA, Giaralis A, Patsialis D. Multi-objective optimal design of inerter-based vibration absorbers for earthquake protection of multi-storey building structures. J Franklin Inst 2019; 356: 7754–84.

[33] Arakaki T, Kuroda H, Arima F, Inoue Y, Baba K. Development of seismic devices applied to ball screw. Part 1: Basic performance test of RD-series. AIJ J Technol Des 1999; 8: 239-44. [in Japanese].

[34] CMC. Code for seismic design of buildings (GB 50011-2010). Beijing: China Ministry of Construction; 2010. [in Chinese].

[35] CMC. Technical specification for concrete structures of tall building (JGJ 3-2010). Beijing: China Ministry of Construction; 2010. [in Chinese].

[36] Ormondroyd J, Den Hartog JP. The theory of dynamic vibration absorber. J Appl Mech – T ASME 1928; 50(7):9.

[37] Den Hartog JP. Mechanical Vibrations. 4th ed. New York: Dover; 1985.

[38] PEER NGA-West2 Database. Pacific Earthquake Engineering Research Center, Report No. 2013/03. Berkeley, CA: University of California, Berkeley, 2013.

[39] Nemhauser GL, Rinnooykan AHG, Todd MJ. Handbooks in operations research and management science. North-Holland; 1989.

[40] Masayoshi N, Hiroto K, Eiji T. Development of real-time pseudo dynamic testing. Earthq Eng Struct Dyn 1992; 21(1): 79-92.

[41] Nakashima M, Masaoka N. Real-time on-line test for MDOF systems. Earthq Eng Struct Dyn 1999; 28(4): 393-420.

[42] ACI (American Concrete Institute). Code requirements for structural concrete (ACI 318-14) and commentary. Farmington Hills, MI: American Concrete Institute; 2014.

[43] Chopra A K. Dynamics of Structures: Theory and Application to Earthquake Engineering. 3rd edition. Upper Saddle River, New Jersey: Pearson Prentice Hall; 2007.

[44] Christopoulos C, Filiatrault A. Principles of passive supplemental damping and seismic isolation. Pavia, Italy: IUSS press; 2006.